JOURNAL OF COMPUTATIONAL PHYSICS 24, 117–132 (1977)

Two-Dimensional Multi-Fluid Tokamak Transport Code*

F. J. HELTON, R. L. MILLER, AND JOHN M. RAWLS

General Atomic Company, P.O. Box 81608, San Diego, California 92138

Received May 6, 1976; revised September 20, 1976

A code is presented which describes the time evolution of axisymmetric plasmas of arbitrary cross section in toroidal geometries. Assuming that flux surface shapes change more slowly than plasma parameters, transport can be regarded as proceeding through a sequence of magnetohydrodynamic equilibria. This assumption suggests an algorithm which involves iteration between one-dimensional transport calculations and two-dimensional equilibrium calculations. Numerical results pertaining to the accuracy of the code and the validity of the algorithm are presented.

1. INTRODUCTION

A number of groups [1] have developed one-dimensional transport codes to describe radial transport in circular cross-section tokamaks. In noncircular cross-section axisymmetric devices, such as doublet or dee machines, the plasma cross section changes in time, necessitating a two-dimensional formulation of the transport problem. However, the physically desirable special case in which the plasma shape changes more slowly than the characteristic plasma parameters (densities, temperatures, magnetic field) can be treated by a quasi static approach. In this formulation transport is regarded as proceeding through a sequence of magnetohydrodynamic equilibria. Hence, the full two-dimensional, time-dependent problem is reduced to a sequence of two-dimensional, time-independent (MHD) calculations interleaved with one-dimensional, time-dependent (transport) calculations using the geometry characterizing the plasma at that time [2].

The transport phase of the algorithm for arbitrary geometry has been cast into a form which closely resembles the standard radial transport code so we begin with a review of the latter in Section 2. In Section 3, the full algorithm for arbitrary geometry is described. Finally, in Section 4, results establishing the accuracy of the code and the validity of the algorithm are presented.

2. THE STANDARD RADIAL TRANSPORT CODE

As mentioned in the Introduction, the transport equations, when averaged over a flux surface of arbitrary cross-sectional shape, can be written in a form which closely

* Work supported by the U. S. Energy Research and Development Administration, Contract No. E(04-3)-167, Project Agreement No. 38.

ISSN 0021-9991

resembles the equation governing the circular cross-section case. Hence, the radial case is briefly reviewed here [3]. The reduction to a one-dimensional code is achieved through the observation that transport along field lines in cases of interest is so much more rapid than transport across field lines that one can regard the plasma variables as constant on flux surfaces. The variables employed are particle density (n), electron temperature (T_e), ion temperature (T_i), and poloidal magnetic field (B_p); their time evolution is described by appropriate moments of the drift kinetic equation and by the poloidal component of Faraday's law. For a low-beta system, these equations can be reduced to a closed set by using Ampere's law,

$$\frac{1}{r}\frac{\partial}{\partial r}(rB_p) = \frac{4\pi}{c} J_\phi , \tag{1}$$

to eliminate the toroidal component of the current **J**, and by using the transport relations,

$$(\text{flux})_m = \sum_n L_{mn}(\text{force})_n , \tag{2}$$

to express the particle and heat fluxes and the toroidal component of the electric field in terms of the basic variables and their radial derivatives. The microscopic physics, i.e., the transport model, enters through the choice of transport coefficients L_{mn} . The resulting set of equations is well understood and has been used to analyze a great variety of phenomena; the principal obstacle in comparing theory with experiment remains the computation of the L_{mn} in realistic physical situations. This problem is aggravated in noncircular geometries.

This system of coupled parabolic nonlinear partial differential equations can be solved by standard difference techniques. In the corresponding equations that arise in the transport phase of the two-dimensional code, we have used a predictor–corrector method with a centered Crank Nicolson scheme (implicit differencing) for both prediction and correction [3, 4]. In the circular cross-section limit, we have applied the code to a standard case [5] previously computed by the Princeton and Texas codes and have found agreement to within 1 %.

The next section discusses the generalizations necessary for calculation of transport in the noncircular case. A transport algorithm for this more general case has been developed and is discussed in some detail. Modules have been attached to this basic framework to include such phenomena as neutral reflux and attenuation, neutral beam injection, and impurity effects, but we discuss here only the algorithm itself.

3. Arbitrary Cross Section

The added complications encountered in the noncircular cross-section problem arise from the more complicated static geometrical description required as well as the fact that the flux surface shapes are generally time dependent. For, in contrast to the circular cross-section case, the flux surface averaged form of Ampere's law

needed to close the transport equations in the general case does not guarantee that Ampere's law is satisfied locally. The problem is thus inherently two-dimensional as well as time dependent. However, as stated above, the assumption that shapes change more slowly than plasma parameters allows the problem to be separated into a sequence of one-dimensional, time-dependent (transport) calculations and two-dimensional, time-independent (equilibrium) calculations. Parameters that are correlated to shape change are monitored during the transport phase and these parameters are used to trigger calls to the equilibrium phase to update the flux surface geometry.

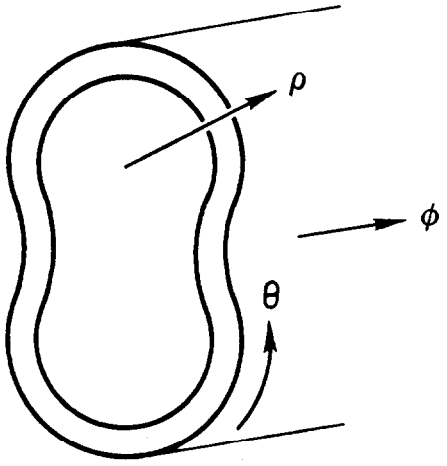

FIG. 1. Coordinate system.

We begin with a brief review of the conventional formalism adopted to describe the magnetics of axisymmetric systems. In the coordinate system illustrated in Fig. 1, the magnetic field takes the form

$$\mathbf{B} = f(\psi)\,\nabla\phi + \nabla\phi \times \nabla\psi, \tag{3}$$

where ψ is the poloidal flux ($\hat{\theta}$ being the poloidal direction). The toroidal and poloidal components of the magnetic field are then, respectively,

$$B_T \equiv B_\phi = f(\psi)/R \tag{4}$$

and

$$B_p \equiv B_\theta = |\,\nabla\psi\,|/R, \tag{5}$$

where R is the radius from the toroidal axis. The toroidal component of Ampere's law may then be written as

$$\Delta^*\psi \equiv \frac{\partial^2\psi}{\partial R^2} + \frac{\partial^2\psi}{\partial z^2} - \frac{1}{R}\frac{\partial\psi}{\partial R} = \frac{4\pi}{c} R J_\phi\,. \tag{6}$$

Since the transport phase of the problem deals only with flux surface averaged quantities, ψ is a possible coordinate. As an alternate to using ψ, we adopt a geometrical coordinate ρ, analogous to the radial coordinate in the circular case, which is defined at a given point to be proportional to the square root of the volume enclosed by the flux surface passing through the point [6]. Explicitly,

$$\rho(\mathbf{x}, t) = \left(\frac{V(\mathbf{x}, t)}{2\pi^2 R_0}\right)^{1/2}, \tag{7}$$

where

$$V(\mathbf{x}, t) \equiv \int_{\psi' < \psi(\mathbf{x},t)} dV = \int (R\, d\phi) \frac{d\psi'}{|\nabla\psi'|} dl_p = 2\pi \int \frac{dl_p}{B_p} d\psi', \tag{8}$$

R_0 is the major radius and dl_p is a line element in the poloidal direction. A description of the numerical techniques used to evaluate the volume integral in Eq. (8) and the surface integrals that appear below is contained in Appendix A.

Written in terms of ρ, the transport equations take on a form for arbitrary geometry very similar to the radial form in the circular cross-section case. Consider first the continuity equation

$$\frac{\partial n(\mathbf{x}, t)}{\partial t} + \nabla \cdot (n\mathbf{u})(\mathbf{x}, t) = 0. \tag{9}$$

As in the radial transport case, the dependence of n on θ and ϕ can be neglected due to the rapid transport along field lines, so that

$$\frac{\partial n(\mathbf{x}, t)}{\partial t} = \frac{\partial n(\rho, t)}{\partial t} + \frac{\partial n(\rho, t)}{\partial \rho} \frac{\partial \rho(\mathbf{x}, t)}{\partial t}. \tag{10}$$

Hence the flux surface average of (9) reads

$$\frac{\partial n(\rho, t)}{\partial t} + \frac{\partial n(\rho, t)}{\partial \rho} \left\langle \frac{\partial \rho(\mathbf{x}, t)}{\partial t} \right\rangle + \frac{1}{\rho} \frac{\partial}{\partial \rho} (\rho \Gamma) = 0 \tag{11}$$

where

$$\Gamma = \langle n\mathbf{u}(x, t) \cdot \nabla\rho \rangle. \tag{12}$$

Here $\langle\ \rangle$ is the usual flux surface average

$$\langle f \rangle = \int \frac{dl_p}{B_p} f \Big/ \int \frac{dl_p}{B_p}, \tag{13}$$

where we have made use of a generalized Gauss law

$$\langle \nabla \cdot \mathbf{A}(\mathbf{x}, t) \rangle = \frac{1}{\partial V/\partial\psi} \frac{\partial}{\partial\psi} \left[\frac{\partial V}{\partial\psi} \langle \mathbf{A}(\mathbf{x}, t) \cdot \nabla\psi \rangle \right], \tag{14}$$

where ψ is any label of the flux surfaces. Equation (11) is further simplified by the observation that the second term vanishes. To see this, consider the lemma

$$\frac{\partial}{\partial t}\int_{R(t)} d^3x\, Q = \int_{R(t)} d^3x \frac{\partial Q}{\partial t} + \int_{\delta R} \mathbf{dS}\cdot\mathbf{u}Q, \tag{15}$$

where $\mathbf{u}$ is the velocity of region R and Q is any function of $\mathbf{x}$ and t. For the case $Q = 1$ and $R(t) =$ the interior of the flux surface at time t which has a fixed volume V, it follows that

$$\langle \mathbf{u}\cdot\nabla V\rangle = \int \mathbf{dS}\cdot\mathbf{u} = 0. \tag{16}$$

The flux surface average of the characteristic equation

$$(\partial V(\mathbf{x}, t)/\partial t) + \mathbf{u}\cdot\nabla V = 0 \tag{17}$$

then implies

$$\langle \partial V(\mathbf{x}, t)/\partial t\rangle = 0, \tag{18}$$

and, of course,

$$\langle \partial\rho(\mathbf{x}, t)/\partial t\rangle = 0. \tag{19}$$

The continuity equation thus reads

$$\partial n/\partial t + (1/\rho)(\partial/\partial\rho)(\rho\Gamma) = 0, \tag{20}$$

just as in the circular cross-section case. The heat flow equations follow the same pattern. The flux averaged form of Faraday's law is written in terms of $\tilde{B}_p$, a flux function analog of the poloidal magnetic field

$$\tilde{B}_p = (1/R_0)(\partial\psi/\partial\rho). \tag{21}$$

Hence B_p can be recovered from $\tilde{B}_p$ via

$$\mathbf{B}_p = (R_0/R)(\boldsymbol{\phi}\times\nabla\rho)\,\tilde{B}_p\,. \tag{22}$$

Since

$$\begin{aligned}\frac{\partial\psi(\rho, t)}{\partial t} &= \left\langle \frac{\partial\psi(\rho, t)}{\partial t}\right\rangle \\ &= \left\langle \frac{\partial\psi(\mathbf{x}, t)}{\partial t}\right\rangle - \frac{\partial\psi(\rho, t)}{\partial\rho}\left\langle \frac{\partial\rho(\mathbf{x}, t)}{\partial t}\right\rangle \\ &= c\langle RE_\phi\rangle,\end{aligned} \tag{23}$$

we have

$$\frac{\partial\tilde{B}_p(\rho, t)}{\partial t} = \frac{1}{R_0}\frac{\partial}{\partial\rho}\left(\frac{\partial\psi(\rho, t)}{\partial t}\right) = \frac{c}{R_0}\frac{\partial}{\partial\rho}\langle RE_\phi\rangle. \tag{24}$$

To summarize, the full set of flux averaged transport equations in the presence of particle and energy source terms reads

$$\begin{aligned}
\frac{\partial n}{\partial t} &= -\frac{1}{\rho}\frac{\partial}{\partial \rho}(\rho \Gamma) + \text{sources},\\
\frac{3}{2}\frac{\partial (nT_e)}{\partial t} &= -\frac{1}{\rho}\frac{\partial}{\partial \rho}(\rho Q_e) + \langle \mathbf{J}\cdot\mathbf{E}\rangle - Q_{ei} - Q_\Gamma + \text{sources},\\
\frac{3}{2}\frac{\partial (nT_i)}{\partial t} &= -\frac{1}{\rho}\frac{\partial}{\partial \rho}(\rho Q_i) + Q_{ei} + Q_\Gamma + \text{sources},\\
\frac{\partial \tilde{B}_p}{\partial t} &= \frac{c}{R_0}\frac{\partial}{\partial \rho}\langle RE_\phi\rangle.
\end{aligned} \tag{25}$$

Here Q_{ei} is the electron–ion thermalization term

$$Q_{ei} = (3n/\tau_e)(m_e/m_p)(T_e - T_i), \tag{26}$$

where

$$\tau_e \equiv 3m_e^{1/2}T_e^{3/2}/[4(2\pi)^{1/2}ne^4 \ln \Lambda], \tag{27}$$

and Q_Γ is an electron–ion energy exchange term which is proportional to the particle flux. The final equation needed is the flux average of the toroidal component of Ampere's law:

$$\begin{aligned}
\langle \nabla\phi \cdot 4\pi \mathbf{J}/c\rangle &= \frac{4\pi}{c}\langle J_\phi/R\rangle\\
&= \langle \nabla\phi\cdot(\nabla\times\mathbf{B})\rangle = \langle \nabla\cdot(\mathbf{B}\times\nabla\phi)\rangle\\
&= \frac{1}{\rho}\frac{\partial}{\partial\rho}(\rho\langle\nabla\rho\cdot(\mathbf{B}\times\nabla\phi)\rangle)\\
&= \frac{1}{\rho}\frac{\partial}{\partial\rho}(\rho\langle|\nabla\rho|B_p/R\rangle),
\end{aligned} \tag{28}$$

or

$$\frac{1}{\rho}\frac{\partial}{\partial\rho}(\kappa\rho\tilde{B}_p) = \frac{4\pi}{c}\langle J_\phi R_0/R\rangle, \tag{29}$$

where

$$\kappa \equiv \langle|\nabla\rho|^2(R_0/R)^2\rangle. \tag{30}$$

To see how the equations close, note that the force–flux relationships in general geometry involve, in addition to the expected quantities $n' \equiv \partial n/\partial\psi$, T_e', T_i', Γ, Q_e, and Q_i, the additional quantities $\langle E_\parallel B\rangle$ and $\langle E_\parallel/B\rangle$ [7]. The ohmic heating term in Eq. (25) also has this property; for the pressure balance relation

$$J_\phi = -cRp' - cff'/4\pi R \tag{31}$$

implies that

$$\langle \mathbf{J}\cdot\mathbf{E}\rangle = -cfp'\langle E_\parallel/B\rangle - cf'\langle E_\parallel B\rangle/4\pi, \tag{32}$$

to lowest order in the inverse aspect ratio. To the same approximation, however,

$$\langle E_\parallel / B \rangle = (1/f)\langle R E_\phi \rangle \tag{33}$$

and

$$\langle E_\parallel B \rangle = f\langle R^{-2} \rangle \langle R E_\phi \rangle \tag{34}$$

so that these combinations involve the same expression which appears in Faraday's law. Thus the equations close in essentially the same manner as in the circular cross-section case.

The two-dimensional equilibrium constraint is then imposed on the above transport equations as follows. An equilibrium calculation is performed to obtain $\rho(x, y)$ and the flux surface average of various quantities at time t_n. Next, transport calculations are carried out for several time steps holding $\rho(x, y)$ fixed. After a given period of time or after certain physical parameters (densities, temperatures, magnetic field) have changed by a specified amount, transport is halted and the resulting current density is used to calculate a new equilibrium. This procedure is illustrated in Fig. 2.

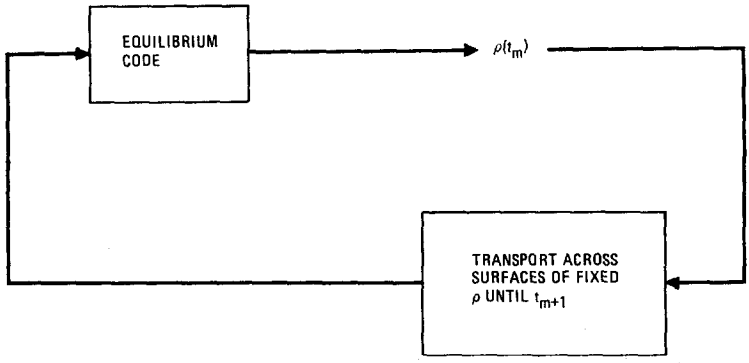

FIG. 2. Algorithm for solution of two-dimensional transport problem.

Having stated the basic ideas behind this approach, we will now explore the algorithm in more detail; refer in the following to the appropriately numbered elements of the flowchart in Fig. 3. We first specify a functional form of the toroidal current (p' and ff'), initial density and temperature profiles, and the boundary conditions {1} for the first equilibrium calculation {2}. We then calculate $\rho(x, y)$ {3}, carry out the relevant flux surface averages and compute the generalized poloidal magnetic field $\tilde{B}_p$ {4}. The transport equations {5} advance the plasma parameters n, T_e, T_i, and $\tilde{B}_p$ in time to t_{m+1}, from which information $\langle J_\phi R_0/R \rangle(\psi, t_{m+1})$ and $p'(\psi, t_{m+1}) = (\partial p/\partial \rho)/(\tilde{B}_p R_0)$ may be recovered {6}. The flux surface average of the pressure balance equation, Eq. (31), is used to compute $ff'(\psi, t_{m+1})$ {7}; the functions p' and ff' so obtained are used to calculate a new equilibrium {8}. The entire procedure is then repeated. The (free boundary) equilibrium module and its application to the problem at hand, specifically how {8} is implemented, are discussed in Appendix B.

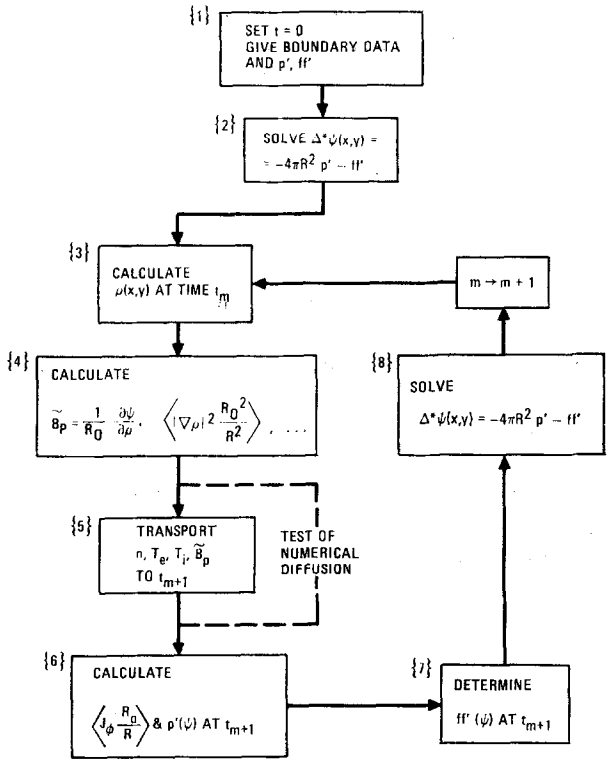

FIG. 3. Flowchart for two-dimensional transport code.

The algorithm as detailed above is still not uniquely defined. For example, an equilibrium calculation results in a pressure profile

$$p' = [n(T_e + T_i)]' \tag{35}$$

differing from that of the preceding transport time step. The initial conditions for the subsequent transport step must then reflect this information but this can be achieved by altering any combination of n, T_e, and T_i.

More generally, it may be remarked that any approach to the problem which does not deal with the full two-dimensional time-dependent nature of the equations is not fully consistent. In the formalism described here, it is explicitly assumed during the transport phase of the calculation that $\langle |\nabla\rho|^2 (R_0/R)^2 \rangle$ is time independent and implicitly assumed that flux surface shapes are time independent. As transport proceeds, these assumptions are violated because of the MHD constraint, Eq. (6). These violations are then manifested as an inconsistency in the algorithm, i.e., the MHD constraint is not strictly satisfied in the transport phase. Further, the constraint is imposed upon the transport solutions in a discontinuous manner during a new

equilibrium calculation (e.g., $\tilde{B}_p$ and some combination of n, T_e, and T_i are altered). The crucial point is then whether these inconsistencies affect the solution. We might expect the solution to be unaffected provided that the flux surface shapes change more slowly than the density, temperatures, and $\tilde{B}_p$ and provided that the MHD constraint is reimposed before strong violation of the constant shape assumption occurs. Evidence is presented in Section 4 which indicates that consistent solutions can in fact be obtained.

4. Verification of the Code

In order to examine the validity of the numerical results, a number of tests have been employed. For example, convegence to a solution is achieved with successive grid refinement and with successive reduction of the transport time steps. In addition, the code has been applied to a very large aspect ratio system with circularly symmetric boundary conditions. In this case, complete agreement is found with the corresponding computation using the one-dimensional radial transport code.

One possible source of error in the algorithm is numerical diffusion arising in large measure from the repeated flux surface averaging of two-dimensional quantities

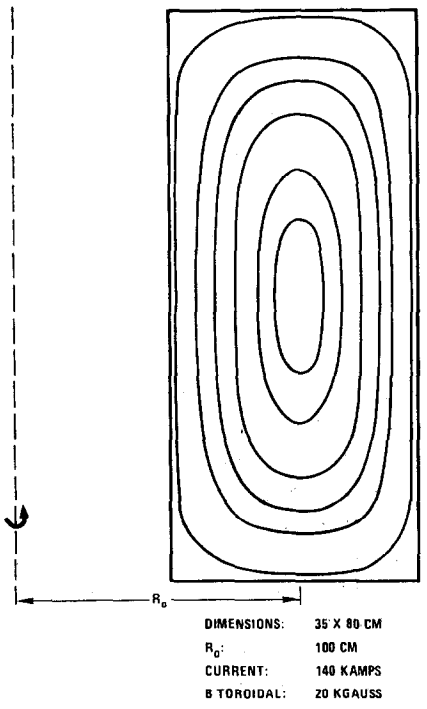

Fig. 4. Plot of contours of constant ψ at $t = 0$.

and the subsequent reconstruction of these 2-D quantities from their flux surface averages. In order to estimate the magnitude of this error, we have performed the iterative calculations involved while bypassing the transport phase (see (Fig. 3). We find that the resulting changes in the various time-dependent quantities are orders of magnitude smaller than the changes found when transport is turned on. In view of the considerable accuracy and numerical stability independently verified in the 1-D transport calculations, we conclude that numerical diffusion is negligible. To reinforce this conclusion by insuring that no cooperative effects between the equilibrium and transport modules induce enhanced numerical diffusion, runs were made in which transport proceeded for only very short time periods; the same results were found.

A second possible source of error is an inability to follow the shape changes that

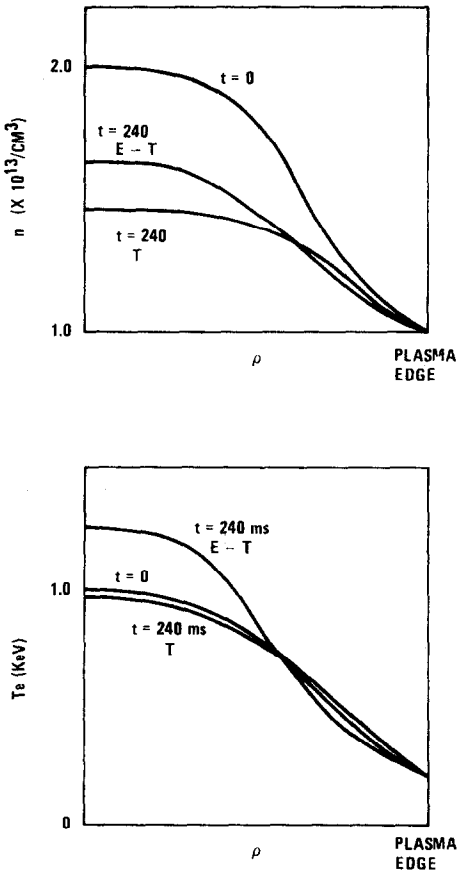

FIG. 5. Plots of electron density and temperature at $t = 0$ and $t = 240$ ms. T refers to the case in which only an initial equilibrium is calculated; $E - T$ refers to the full equilibrium–transport calculation.

of necessity accompany transport in noncircular geometries. A convenient check on the accuracy with which $\rho(x, y)$ is followed in time is the geometrical theorem Eq. (19). In our numerical results, $\langle \partial\rho/\partial t \rangle$ is typically two orders of magnitude smaller than $\langle | \partial\rho/\partial t | \rangle$, a quantity which is itself usually smaller than might be expected from Eq. (11), i.e., $(\partial n/\partial t)/(\partial n/\partial \rho)$. This result is a positive indication that changes in shape are being followed accurately.

Of more significance to the validity of the algorithm employed here is that convergence should be achieved as the criterion for terminating transport and computing another equilibrium is made more stringent. For consistency, a sequence of runs with

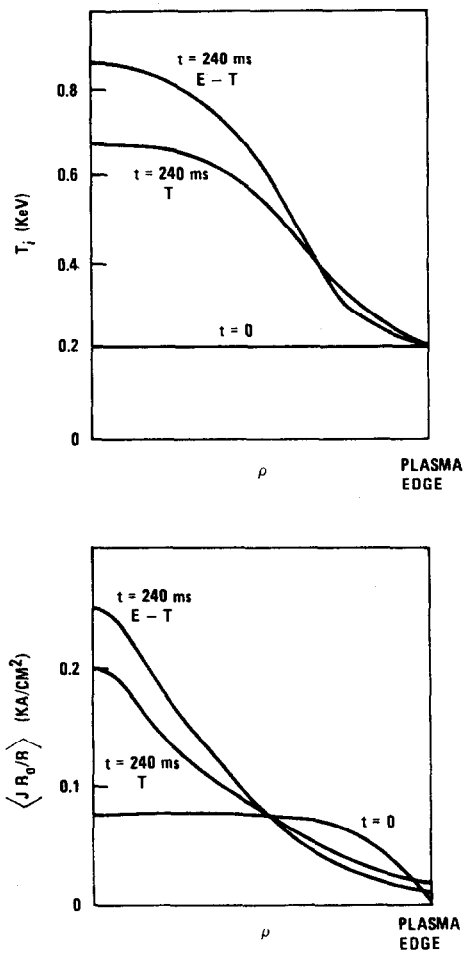

FIG. 6. Plots of ion temperature and current density at $t = 0$ and $t = 240$ ms. T refers to the case in which only an initial equilibrium is calculated; $E - T$ refers to the full equilibrium–transport calculation.

an increasing frequency of calls to the equilibrium module should converge to the solution of the full 2-D time-dependent problem.

Convergence should also be obtained regardless of the manner in which n, T_e, and T_i are made consistent with Eq. (35) as discussed in Section 3. To demonstrate the convergence properties, an illustrative case is presented with the initial equilibrium shown in Fig. 4. The initial current density profile is taken to be

$$J = (J_0/2)((R/R_0) + (R_0/R)) \tag{36}$$

and initial particle density, current density, and temperature profiles are shown in Figs. 5 and 6. The particle diffusion coefficient and the electron thermal conductivity obey pseudoclassical scaling laws while the ion thermal conductivity is neoclassical. By pseudoclassical and neoclassical, we mean here the usual scaling laws written in terms of the generalized poloidal field $\tilde{B}_p$ rather than in terms of B_p; no attempt has been made to justify this form for the transport coefficients. The boundary conditions imposed on the runs are fixed edge density and temperatures, and fixed total current.

Transport proceeds for 240 miliseconds (corresponding to about 60 transport time steps) in 4 different runs. In the first case, $N(60)$, no equilibria are calculated after the initial one and hence no correction for shape change is ever made. In the second case, $N(5)$, a new equilibrium is calculated every 5 time steps and the density is then readjusted subject to the new $p(\rho)$ and Eq. (35). The third case, $N(2)$, also readjusts the density but a new equilibrium is calculated every 2 time steps. In the final case, $T(5)$, a new equilibrium is calculated every 5 time steps but T_e and T_i are readjusted, maintaining T_e/T_i constant, after every equilibrium calculation. The convergence of these runs is demonstrated in Table I by listing the peak values of the density, temperatures, and current after 240 msec for each case.

TABLE I

Central Values of the Plasma Parameters

	n (10^{13}/cm^3)	T_e (kev)	T_i (kev)	J (kamps/cm^2)
$N(60)$	1.52	0.97	0.73	0.183
$N(5)$	1.68	1.23	0.87	0.248
$N(2)$	1.69	1.26	0.88	0.251
$T(5)$	1.69	1.27	0.90	0.251

Finally, the resulting profiles of n, T_e, T_i, and current density are shown in Figs. 5 and 6 and the shape of the flux surfaces after 240 msec is shown in Fig. 7. The shape change is evident by comparison with Fig. 4.

From the evidence presented in this section, it is concluded that the algorithm does accurately describe the time evolution of plasma profiles in the general geometry case, provided the geometry does not change too rapidly on the transport time scale.

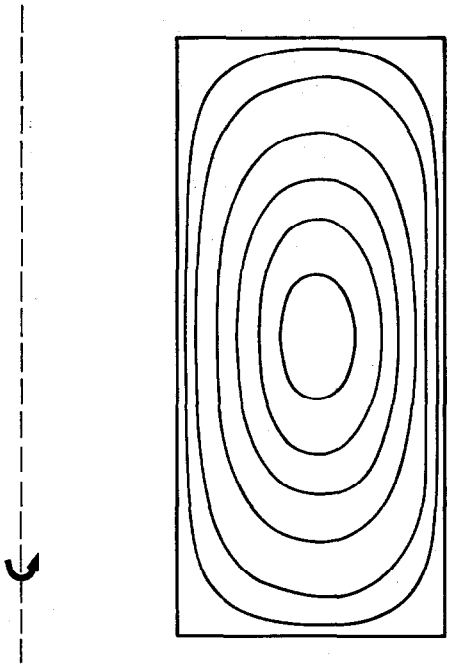

FIG. 7. Plots of contours of constant ψ at $t = 240$ ms.

The restriction to slow shape changes appears to impose practical limitations on the applicability of the code; for example, the accurate description of startup phenomena or of doublet–droplet transformations appears to be precluded. In any case, the algorithm in its present state of development cannot yet deal with singular surfaces such as a separatrix. A separate analytic formalism is required in the neighborhood of such a surface because the equations themselves develop singularities.

APPENDIX A

In this appendix, we describe the numerical procedures employed to evaluate the integrals that arise in the algorithm. The calculation of integrals over (or interior to) a flux surface requires a determination of that flux surface contour from the values of ψ that emerge from the equilibrium module, i.e., $\psi(x, y)$ on a rectangular mesh. This is accomplished by a line-tracing routine which uses four-point interpolation in ψ to determine x (or y) and $|\nabla\psi|^2$ at each point the ψ contour crosses a y (or x) mesh line. The set of coordinates (x_i, y_i) so generated is then used to define a monotone parameter

$$t_i = \sum_{j=1}^{i} [(x_{j+1} - x_j)^2 + (y_{j+1} - y_j)^2]^{1/2} \tag{A.1}$$

which is useful for parametric integration [8]. In particular the computation of $\rho(x, y)$ is found from

$$\begin{aligned} V(x, y) &= 2\pi^2 R_0 \rho^2[\psi(x, y)] = \int_{\psi<\psi(x,y)} R\, dR\, dy\, d\phi = 2\pi \int (R_0 + x)\, dx\, dy \\ &= 2\pi R_0 \int y\, dx + \pi \int y\, d(x^2) \\ &= 2\pi R_0 \int dt\, y(t)(dx/dt) + \pi \int dt\, y(t)(dx^2/dt). \end{aligned} \tag{A.2}$$

Flux surface averaging is carried out in a similar fashion:

$$\begin{aligned} \langle A \rangle &= \int \frac{dl_p}{B_p} A \Big/ \int \frac{dl_p}{B_p} \\ &= \int dt\, \frac{A(t)\, R(t)\, l(t)}{|\nabla\psi(t)|} \Big/ \int dt\, \frac{R(t)\, l(t)}{|\nabla\psi(t)|}, \end{aligned} \tag{A.3}$$

where

$$l(t) = [(dx/dt)^2 + (dy/dt)^2]^{1/2}.$$

The integrands are then obtained as polynomials in t from four-point interpolation formulas, and so the remaining integral can be performed analytically.

Near the magnetic axis, a scarcity of mesh points prevents accurate integration by the above method. In this near axis region both extrapolation techniques and expansion techniques have been used.

Appendix B

Here we present the method used to obtain a new equilibrium from the p' and ff' values that are computed from the results of a transport calculation. We seek a solution to

$$\Delta^*\psi = -4\pi R^2 p'(\psi) - ff'(\psi) \tag{B.1}$$

subject to the constraint that the total current I is held fixed. The major difficulty with this calculation is that p' and ff' are known only in tabular form (see Table B-1)

TABLE B-1

Table of p' and ff' Resulting from Transport Calculation

ψ	p'	ff'
$\psi^0_{\min}$	p_1'	$(ff')_1$
$\psi^0_{\min} + d\psi^0$	p_2'	$(ff')_2$
⋮	⋮	⋮
$\psi^0_{\max} = \psi^0_{\min} + (N-1)\, d\psi^0$	p_N'	$(ff')_N$

and not as analytic functions of ψ. This means that any attempt to solve Eq. (B.1) iteratively [9] will entail reinterpretation of Table B-1 after each iteration. Specifically, after the first iteration,

$$\Delta^*\psi^1 = -4\pi R^2 p'(\psi^0) - ff'(\psi^0), \tag{B.2}$$

we find that

$$\begin{aligned} \psi^1_{\max} &\neq \psi^0_{\max}, \\ \psi^1_{\min} &\neq \psi^0_{\min}, \end{aligned} \tag{B.3}$$

and

$$\psi^1_{\max} - \psi^1_{\min} \neq \psi^0_{\max} - \psi^0_{\min},$$

where $p'(\psi^0)$ and $ff'(\psi^0)$ are obtained from interpolation of Table B-1. During each iteration, $\psi_{\max}$ is the value of the poloidal flux on the largest flux surface which does not intersect a specified limiter surface; the current outside this flux surface is scraped off. To proceed to the next iteration we adopt the translation

$$\begin{aligned} \psi^n_{\min} &\to \psi^{n+1}_{\min}, \\ \psi^n_{\max} &\to \psi^{n+1}_{\max}, \\ d\psi^n &\to (\psi^{n+1}_{\max} - \psi^{n+1}_{\min})/(N-1), \end{aligned} \tag{B.4}$$

where n is the iteration number.

The constant current constraint can be maintained in this procedure by defining

$$\alpha^n = I \Big/ \left\{ -c \int dA(Rp' + ff'/4\pi R) \right\} \tag{B.5}$$

and then rescaling p' and ff' after each iteration by

$$\begin{aligned} p_i' &\to \alpha^n p_i', \\ (ff')_i &\to \alpha^n (ff')_i, \qquad i = 1,\ldots, N. \end{aligned} \tag{B.6}$$

In practice this scheme converges rapidly and we find for all n

$$\begin{aligned} \alpha^n &\approx 1.00, \\ \psi^{n+1}_{\max} &\approx \psi^n_{\max}, \\ \psi^{n+1}_{\min} &\approx \psi^n_{\min}. \end{aligned} \tag{B.7}$$

ACKNOWLEDGMENT

It is a pleasure to acknowledge many valuable discussions with Professor F. L. Hinton of the University of Texas at Austin.

REFERENCES

1. J. T. HOGAN, "Multi-Fluid Tokamak Transport Models," ORNL-TM-5153 *in* "Methods in Computational Physics," Volume 16: Computer Applications to Controlled Fusion Research, pp. 131–164.
2. The separation of the problem into 1-D and 2-D elements, with the coupling provided by functions of the shapes of the surfaces, was first put forward by H. Grad in Oak Ridge memos dated April 22 and July 6, 1970.
3. J. C. WILEY, "Numerical Simulation of the Radial Neoclassical Transport Equations," Ph.D. Thesis, University of Texas, Austin, 1974.
4. R. D. RICHTMYER AND K. W. MORTON, "Difference Methods for Initial Value Problems," Wiley, New York, 1967.
5. F. L. HINTON, J. C. WILEY, D. F. DUCHS, H. P. FURTH, AND P. H. RUTHERFORD, *Phys. Rev. Lett.* **29** (1972), 698.
6. F. L. HINTON suggested the use of the ρ-coordinate to us and pointed out its merits.
7. R. D. HAZELTINE, F. L. HINTON, AND M. N. ROSENBLUTH, *Phys. Fluids* **16** (1973), 1645.
8. D. C. STEVENS, private communication.
9. O. BUNEMAN, "A Compact Non-Iterative Poisson Solver," SUIPR Report No. 294, Stanford University, May 1969.